
Large-Batch, Neural Multi-Objective Bayesian Optimization

Navid Ansari

Max Planck Institute for Informatics
Saarbrücken, Germany
nansari@mpi-inf.mpg.de

Hans-Peter Seidel

Max Planck Institute for Informatics
Saarbrücken, Germany
hpseidel@mpi-sb.mpg.de

Vahid Babaei

Max Planck Institute for Informatics
Saarbrücken, Germany
vbabaei@mpi-inf.mpg.de

Abstract

Bayesian optimization provides a powerful framework for global optimization of black-box, expensive-to-evaluate functions. However, it has a limited capacity in handling data-intensive problems, especially in multi-objective settings, due to the poor scalability of default Gaussian Process surrogates. We present a novel Bayesian optimization framework specifically tailored to address these limitations. Our method leverages a Bayesian neural networks approach for surrogate modeling. This enables efficient handling of large batches of data, modeling complex problems, and generating the uncertainty of the predictions. In addition, our method incorporates a scalable, uncertainty-aware acquisition strategy based on the well-known, easy-to-deploy NSGA-II. This fully parallelizable strategy promotes efficient exploration of uncharted regions. Our framework allows for effective optimization in data-intensive environments with a minimum number of iterations. We demonstrate the superiority of our method by comparing it with state-of-the-art multi-objective optimizations. We perform our evaluation on two real-world problems - airfoil design and color printing - showcasing the applicability and efficiency of our approach. Code is available at: https://github.com/an-on-ym-ous/lbn_mobo

1 Introduction

Design of objects and materials that lead to a specific *performance*, typically defined by multiple objectives, is a long-standing, critical challenge in engineering [4]. Oftentimes, in real-world applications the forward mechanism that govern the design processes are expensive to evaluate, whether they are sophisticated physics-based simulations or time- and labor-intensive lab experiments. We call these underlying mechanisms *Native Forward Processes* or NFP. An elegant solution to these design optimization problems is the *online* sampling of the NFP through informed guesses about the best samples at each iteration. Particularly, Bayesian optimization [21] is a powerful paradigm featuring a *surrogate* model that gets updated iteratively using a single data point or a small batch of data at each iteration. The choice of the next-iteration data is through optimizing a so-called *acquisition* function.

In recent years, an *offline* problem setup called model-based design [14, 33] has emerged where iterative sampling of the NFP is considered non-viable. Model-based design assumes that while there exists a typically large but fixed set of NFP samples, the NFP itself is not easily available. Consider, for example, the dataset of 21263 superconductor materials annotated with their critical temperature

[17]. There is however another class of design problems that lies in between online and offline setups. In this setting, iterative sampling of large batches of data is possible but with a minimal number of iterations. A low number of iterations is highly desirable because creating new batches of samples can be expensive. Nevertheless, we can include a large number of samples in a single batch at almost no additional cost. For example, the startup cost of 3D printing a single, small object and many of its instances that fit the build volume, is almost identical [16]. This setup, especially for design problems, is under-represented in the literature. Existing methods have limitations in retrieving good solutions either in a few generations, or handling very large training data, or dealing with multiple objectives.

To address these limitations, we propose large-batch, neural multi-objective Bayesian optimization (**LBN-MOBO**). Our method has two key components. i) We use a neural network ensemble as the surrogate. This surrogate enables handling very large batches of data and also computing predictive uncertainty. ii) We propose a highly practical acquisition function based on multi-objective sorting of samples where not only the performance objective but also its associated uncertainty is considered when ranking the samples.

Our proposed method offers a set of important advantages. First, it can retrieve a dense *Pareto front*, capturing the trade-off between multiple objectives, at each iteration which results in convergence in as few iterations as possible. Second, it can handle very large training data, enabling it to be applied to a wide range of engineering problems including those arising from high-dimensional design spaces. Third, it is highly parallelizable, shifting the bottleneck from the BO algorithm to the computational infrastructure or experimentation capacities used to evaluate the NFP. We demonstrate the effectiveness of our proposed method through experiments on several benchmark problems, showing that it outperforms existing methods in terms of convergence in a small number of generations.

2 Related work

To the best of our knowledge there exist no method that can handle very large data batches for multi-objective optimization while leveraging high-capacity, uncertainty-aware surrogate models such as Bayesian neural networks (BNNs). There are however many methods that possess one or some of the above mentioned features. In this section we introduce some of the main competitors and in Section 4 we evaluate their performance and analyze their limitations. For an effective comparison, the methods must at least possess two characteristics. First, they must be capable of managing multi-objective optimizations. Second, they must handle a moderately large batch size.

Non-dominated sorting genetic algorithm II (NSGA-II) [11] is an exceptionally popular method for multi-objective optimization. It belongs to multi-objective evolutionary algorithms (MOEA), which have been applied to a variety of problems, from engineering [26] to finance [30]. Despite their widespread use, MOEA have certain limitations. One major challenge is the computational cost of MOEAs, as they typically require a large number of function evaluations to converge to a good solution [22]. This can make MOEAs impractical for problems with computationally expensive objective functions or high-dimensional design spaces. Moreover, they are prone to trap in local minima. This can be particularly problematic for problems with multiple local optima or non-convex objective functions.

Bayesian optimization (BO) is adept at efficiently searching for the global optimum while minimizing the number of function evaluations [21]. However, extending BO to multi-objective batch optimization is not straightforward. **USEMO** [5] is one of the state of the art extensions of BO that is capable of solving multi objective problems. It employs NSGA-II to identify the Pareto front on the surrogate and uses uncertainty information to select a subset of candidates for the next iteration. **TSEMO** [7] takes a different approach by using Thompson sampling and NSGA-II on Gaussian process (GP) surrogates to find the next batch of samples that maximize the hypervolume. However, these methods struggle to maintain diversity and fail to capture part of the final Pareto front[22].

Diversity-guided multi-objective Bayesian optimization (DGEMO) seeks to address this issue by dividing the performance and design spaces into diverse regions and striving to identify candidates in as diverse locations as possible while maintaining the performance [22]. However, its computational time grows exponentially with the increase in batch size.

BO methods face a bottleneck when given large batch sizes as they typically use Gaussian processes as surrogate models. When dealing with large batches of data, neural networks (NNs) come as suitable fits for modeling the problems. There have been several attempts to replace GPs with NNs, but to provide uncertainty information, approximations of Bayesian neural networks are required. In this regard, [29] applies adaptive basis function regression with a neural network to approximate uncertainty and uses neural Bayesian optimization for various single-objective optimizations. Similarly, [13] uses Deep Ensembles [23] and dropout [15] to estimate uncertainty and applies the resulting Bayesian optimization on a graph neural network to generate designs with improved performance. These methodologies all focus on a single objective and don't yield a Pareto front. One significant challenge, which we address in this work, is to devise an appropriate acquisition function that can generate a diverse set of Pareto front candidates without causing computational inefficiencies in the overall process.

3 Method

Our method, LBN-MOBO, is an easy to deploy optimization framework adept at multi-objective optimization, capable of exploring large design spaces, managing considerably large data batches, and reaching convergence in a minimal number of iterations (Section 3.1). This robust functionality is made possible by two primary components. First, instead of traditional Gaussian processes (GPs), we leverage neural networks (NNs) as surrogate models. NNs, unlike GPs, have extreme capacity in managing large training data [18], making them an ideal solution for modeling complex problems [10, 19]. More specifically, we use a neural-network surrogate model capable of estimating the (epistemic) uncertainty, a critical factor in LBN-MOBO's second component (Section 3.2).

The second component of LBN-MOBO is a scalable and uncertainty-aware acquisition function (Section 3.3). This function generates the candidate designs for the subsequent iterations. By bringing in the uncertainty as an additional objective, LBN-MOBO can explore previously unseen regions, preventing it from getting trapped in local minima. This acquisition function is fully parallelizable. Given sufficient parallel computational resources for evaluating the NFP, LBN-MOBO scales gracefully with the batch size, allowing for efficient optimization even with large data.

3.1 Large-batch neural multi-objective Bayesian optimization (LBN-MOBO)

Bayesian optimization for optimizing black-box NFP Φ , uses a surrogate model to create a prior over the objective function, which is updated with each new observation. An acquisition function A_F , derived from the surrogate model, guides the selection of the next sample, balancing exploration and exploitation. After evaluating the sample's performance, the surrogate model is updated. The process continues until a predetermined stopping criterion is reached.

Our method, LBN-MOBO, works on the same principles but devised to achieve scalability. LBN-MOBO begins with a random sampling of the design space $U_S(\mathcal{X})$ of the given NFP Φ . Subsequently, it fits a Bayesian neural network surrogate f_{BNN} to the randomly sampled dataset \mathbf{X}^0 in order to handle larger training data. Additionally, the Bayesian neural network f_{BNN} , and particularly its approximation through Deep Ensembles [23], enables computing predictive uncertainties ($\mathbb{F}_\sigma(\mathbf{x})$) in a fully parallelized manner (Section 3.2). Upon training f_{BNN} , we utilize our acquisition function (A_F) to compute the $2mD$ Pareto front, which explores both promising and under-represented regions (Section 3.3). We append the calculated candidates to our data and utilize the updated dataset to train the BNN for the next generation.

Figure 1 illustrates the stages of the LBN-MOBO algorithm using two objectives as an example. Observe that some of the candidates may not be positioned on the Pareto front of the NFP (indicated by the red regions), but they are still retained in the data set. This is because they contribute to enhancing the information of f_{BNN} and decreasing its uncertainty level ($\mathbb{F}_\sigma(\mathbf{x})$). Algorithm 1 provides a concise summary of all the steps of LBN-MOBO.

3.2 Bayesian neural network surrogate f_{BNN}

In this work, we employ a modified version of Deep Ensembles [23] as an approximation of a BNN [29]. Deep Ensembles consist of an ensemble of K neural networks, \hat{f}_k , each capable of providing a

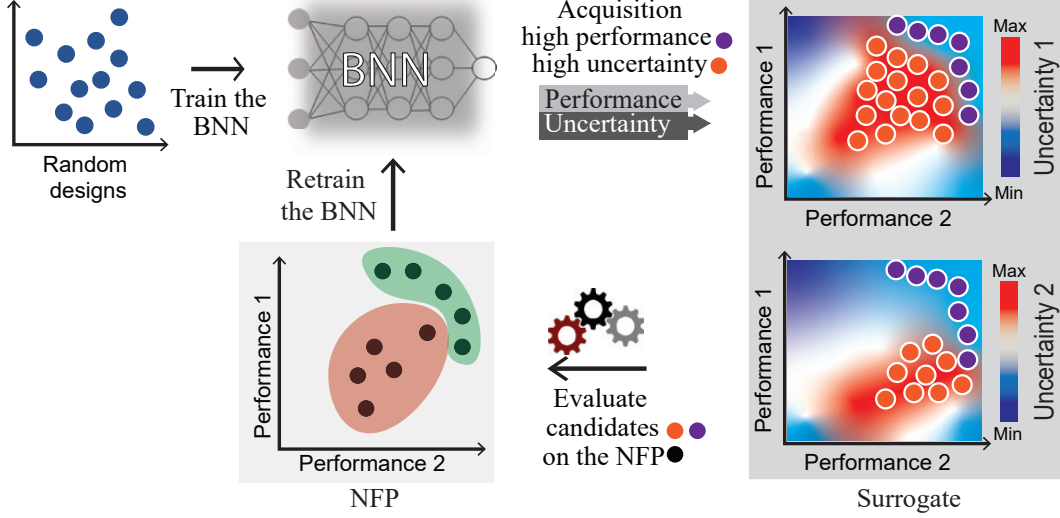


Figure 1: LBN-MOBO starts with training a Bayesian neural network (f_{BNN}) on random designs. We then run our acquisition function (A_F) and compute a 2MD Pareto front to explore promising (green) and under-represented regions (red) of the NFP. We then append the acquired candidates to the data set and retrain f_{BNN} . By incorporating uncertainty information alongside the Pareto front of the best performances (blue candidates), we identify promising candidates in areas of high uncertainty, where there is potential for additional information (red candidates).

prediction $\mu_k(\mathbf{x})$ and its associated *aleatoric* uncertainty $\sigma_k(\mathbf{x})$ in the form of a Gaussian distribution $\mathcal{N}(\mu_k(\mathbf{x}), \sigma_k(\mathbf{x}))$.

In our case, in order to guide our optimizer to explore under-represented regions, we only require *epistemic* uncertainty. This is because the epistemic uncertainty is higher in areas where the networks in the ensemble fit differently due to a lack of information.

Thus, we only train K neural networks using the traditional mean squared error (MSE) loss.

$$\mathcal{L}_k^{MSE} := (\mathbf{y}^* - \mu_k(\mathbf{x}))^2. \quad (1)$$

Next, we extract the epistemic uncertainty $\mathbb{F}_\sigma(\mathbf{x})$ from the networks in the ensemble:

$$\mathbb{F}_\mu(\mathbf{x}) := \frac{1}{K} \sum_k \mu_k(\mathbf{x}), \quad (2a)$$

$$\mathbb{F}_\sigma(\mathbf{x}) = \frac{1}{K} \sum_k (\mu_k^2(\mathbf{x}) - \mathbb{F}_\mu^2(\mathbf{x})). \quad (2b)$$

Next, we show how epistemic uncertainty enables exploration in acquisition function (A_F).

3.3 2MD acquisition function

An acquisition function should predict the worthiest candidates for the next iteration of the Bayesian optimization [27]. This translates to not only selecting designs with high performance on the surrogate model but also considering the uncertainty of the surrogate model. Candidates in uncertain regions of the surrogate model may contain appropriate solutions and a powerful acquisition function should be able to explore these regions effectively. Several popular acquisition functions such as Expected Improvement [21] and Upper Confidence Bound [8] operate on this principle.

Without the loss of generality, we assume a problem that seeks to maximize performance objectives. Our acquisition strategy employs the widely-used NSGA-II [11] and specifically its multi-objective non-dominated sorting method that finds the Pareto front of the surrogate at a given iteration of LBN-MOBO. The key insight of our acquisition method is that instead of finding an M dimensional

ALGORITHM 1: Large-batch, neural multi-objective Bayesian optimization (LBN-MOBO).

Input

S // Batch size
 Q // Number of iterations of the main algorithm
 \mathcal{X} // $\mathcal{X} \in \mathcal{R}^n$, n dimensional design space
 Φ // Native Forward Process, e.g., a simulation

Process parameters

$f_{BNN}(\mathcal{X})$ // Bayesian neural surrogate

Output

P_S, P_F // Pareto set (designs) and Pareto front (performances) of the NFP

begin

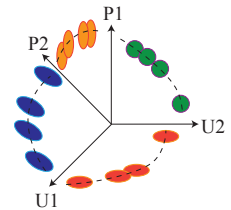
```
// Draw  $S$  random samples from the design space.  
 $\mathbf{X}^0 \leftarrow \mathbf{U}_S(\mathcal{X})$   
// Query  $\Phi$  and form the data set.  
 $\mathbf{Y}^0 \leftarrow \Phi(\mathbf{X}^0)$   
 $dataset \leftarrow (\mathbf{X}^0, \mathbf{Y}^0)$   
 $f_{BNN}^0 \xleftarrow{\text{train}} dataset$  // Train the BNN surrogate.  
for  $i \leftarrow 1$  to  $Q$  do  
   $P_S^i \leftarrow A_F(f_{BNN}^{i-1}, S)$   
   $P_F^i \leftarrow \Phi(P_S^i)$  // Calculate the performance on the NFP.  
   $dataset \leftarrow (P_F^i, P_S^i)$  // Append new data to the old.  
   $f_{BNN}^i \xleftarrow{\text{train}} dataset$  // Train the BNN surrogate.  
end  
end
```

Pareto front corresponding to M objectives (each given by $\mathbb{F}_\mu^m(\mathbf{x})$, $m \in [1, M]$), it finds a $2M$ dimensional Pareto front where M dimensions correspond to performance objectives and the other M dimensions correspond to the uncertainty of those objectives (each given by $\mathbb{F}_\sigma^m(\mathbf{x})$, $m \in [1, M]$). In other words, our acquisition function A_F *simultaneously* maximizes the predicted objectives and their associated uncertainties (both given by our surrogate f_{BNN}):

$$A_F := \arg \max_{\mathbf{x}} \{ \mathbb{F}_\mu^m(\mathbf{x}), \mathbb{F}_\sigma^m(\mathbf{x}) \}, m \in [1, M]. \quad (3)$$

Note that in practice NSGA-II experiences a sample size bottleneck and struggles to scale effectively as the population expands. To overcome this limitation, we employ in parallel independent acquisitions (different NSGA-II seeds) with smaller batch sizes, and combine the results. Ultimately, similar to our surrogate model, our acquisition function (A_F) is fully parallelizable, and its performance remains unhampered even when batch size increases. Consequently, the sole limiting factor for executing LBN-MOBO is our parallel processing capability when querying the NFP.

Let us provide the intuition behind our acquisition strategy. The inset figure provides a schematic four-dimensional acquisition function A_F . Clearly, we want to evaluate the orange samples, currently evaluated only on the surrogate, on the NFP as they are suggested by A_F to be dominant in at least one *performance* dimension (P1 or P2). On the other hand, the blue, red, and green samples are chosen partially or entirely due to their high uncertainty in at least one dimension (U1 or U2). These samples correspond to unexplored regions in the design space. They are beneficial in two ways: either they prove to be part of the Pareto front once being evaluated on the NFP, or they contribute to filling the gap between the surrogate and the NFP, leading to a more informative surrogate model. This enhances the quality of the surrogate model,



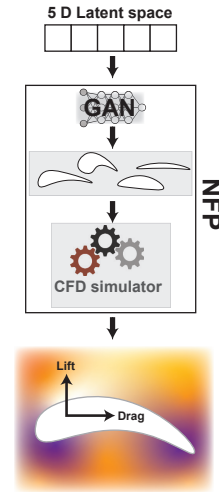
making it as similar as possible to the NFP, thereby improving its predictive power for subsequent iterations.

4 Evaluation

4.1 Experiments

ZDT3 refers to one of the problems in the Zitzler-Deb-Thiele (ZDT) test suite [35]. The ZDT test suite is a set of benchmark functions widely used to evaluate and compare the performance of multi-objective optimization algorithms. ZDT3 specifically consists of two objectives and a disjoint Pareto front. The equations of objectives as well as additional evaluations using other test suits are available in the supplementary materials.

Airfoil represents, for example, the cross-sectional shape of an airplane wing, with its performance quantified by the lift coefficient C_L and the lift-to-drag ratio C_L/C_D [25]. The aim of this experiment is to explore different airfoil shapes to discover the Pareto front of these performances (C_L and C_L/C_D). Lift is the upward force that acts perpendicular to the direction of incoming airflow, primarily serving to counterbalance the weight of an aircraft or providing an upward thrust for an airfoil. Drag is the resistance encountered by an object as it moves through a fluid. It acts in the opposite direction to the free stream flow and parallel to it. Minimizing the drag is important for maximizing the efficiency and speed of vehicles, as well as reducing fuel consumption. In standard computational fluid dynamics (CFD) simulations, the Navier-Stokes equations are solved around the airfoil to compute C_L and C_L/C_D . We utilize the open-source software OpenFOAM for running our simulations, setting the free stream angle to 0 and length to 40 [24, 32]. The design parameters of this problem describe the shape of the airfoils. Due to high dimensionality and complex shape constraints, we employ a specific type of Generative Adversarial Networks (GANs) to transform the complex design space into a manageable five-dimensional latent space [9]. We assess the shapes generated by GAN using a Computational Fluid Dynamics (CFD) simulator to measure the values of C_L and C_L/C_D . As such, our NFP in this problem is a combination of the GAN and the CFD simulator (inset).



Printer’s color gamut. A color gamut represents the range of colors that can be achieved using a specific device, such as a display or a printer [34]. In this experiment, we compute the color gamut of a printer by determining the Pareto front of a multi-objective optimization problem. A printer combines different amounts of its limited number of inks to create a range of colors. The design parameters of this problem are the amount of available inks. We explore CIEa*b* color space [20] which is our performance space. CIE a* represents the color-opponent dimension of red-green, with negative values representing green and positive values representing red. CIE b* represents the color-opponent dimension of blue-yellow, with negative values representing blue and positive values representing yellow.

Following [3] we create a printer NFP using an ensemble of 10 neural networks (not related to our ensemble surrogate). We create a complex instance of this problem where we simulate a printer NFP with 44 inks [2]. All networks in the ensemble NFP are trained on 344,000 printed patches with varying ink-amount combinations and their corresponding a*b* colors. This problem has a 44 dimensional design space as the printer NFP assumes 44 inks.

4.2 Benchmarking LBN-MOBO on ZDT3

In this study, we highlight the superior performance of the LBN-MOBO compared to a set of state-of-the-art Multi-objective Bayesian optimizations, namely USEMO, DGEMO, TSEMO, and NSGA-II, on the ZDT3 test. We demonstrate how LBN-MOBO adeptly manages large design spaces while maintaining a significantly shorter optimization time compared to its counterparts. This investigation involves two ZDT3 problem configurations. The first experiment focuses on a 6-dimensional design space, while the second broadens this space to 30 dimensions, thereby increasing the complexity of the search space. We maintain a fair comparison by limiting the batch size to 1000 samples for all algorithms despite the fact that LBN-MOBO inherently possesses the ability to handle much

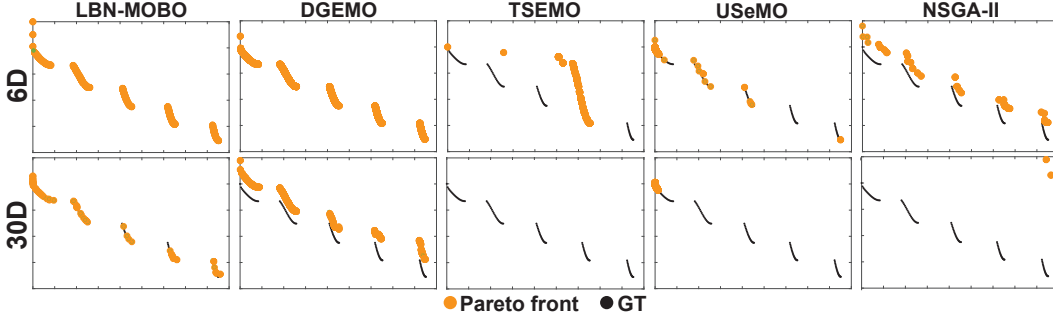


Figure 2: Obtained Pareto front by different methods on 6 dimensional and 30 dimensional ZDT3 problem. Batch size for all experiments is fixed at 1000.

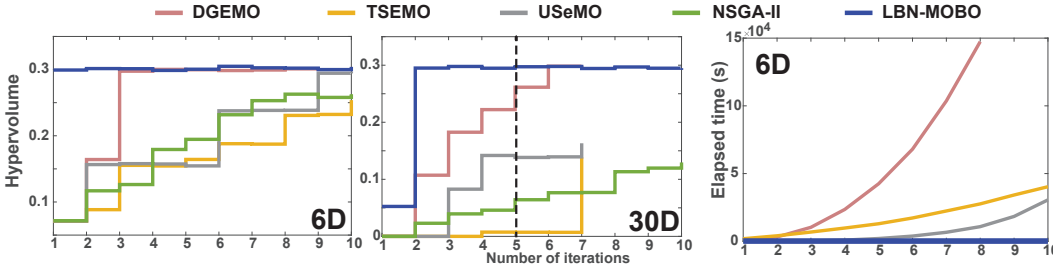


Figure 3: The left and middle plot represent the hypervolume of the 6 and 30 dimensional ZDT3 problem, respectively. The plot on the right shows the elapsed time for 6D problem for all methods (the NSGA-II plot is masked under LBN-MOBO).

larger batches. Using 1000 samples is an approximate limit of tractability for most of the competing methods. Moreover throughout this experiment we use an equal number of iterations for all methods, except in cases where a method becomes intractable due to unmanageable computational load.

Figure 2 (top) shows the superior performance of LBN-MOBO and DGEMO in contrast with the other algorithms for the 6-dimensional ZDT3 problem. In this figure, the illustrated Pareto fronts are the final results of 10 optimization iterations. When confronted with the 30 dimensional problem (bottom row), the optimization methods must navigate a significantly larger space within the same sampling constraints. For this problem, we have shown the results of optimizations at iteration 5.

In Figure 3 (left and middle), we further clarify the performance of different methods by showing the evolution of the hypervolume of the Pareto front at each iteration. For the 6D problem, LBN-MOBO manages to find the Pareto front after a single iteration. For the 30D problem, LBN-MOBO finds the Pareto front after two iterations and maintains its dominance over the other methods until the 6th iteration where DGEMO reaches it. We note that to approximate the hypervolume, we employed [28] that uses random sampling. As a result, occasional minor fluctuations may arise. It's worth mentioning that for the 30D problem we were unable to complete 10 iterations for UseMO, TSEMO, and DGEMO due to their exponential rise in computational time.

Figure 3 (right) depicts the run-time of all methods for 6D ZDT3 for 10 iterations. Even in this fairly straightforward problem, the computational time for UseMO, TSEMO, and particularly DGEMO surged dramatically. Conversely, the total computational time for NSGA2 was less than 14 seconds. The last and longest iteration of LBN-MOBO was 167s for training the ensemble models and 13.5s for acquisition.

4.3 LBN-MOBO for real-world problems

In this study, we put the capabilities of LBN-MOBO into practice for two real-world complex problems: airfoil and printer's color gamut, employing LBN-MOBO with larger batch sizes of 15,000 and 20,000, respectively. We compare our method against NSGA-II, as it is the sole method capable of managing a batch sizes of 20,000. Additionally, we consider DGEMO due to its competitive

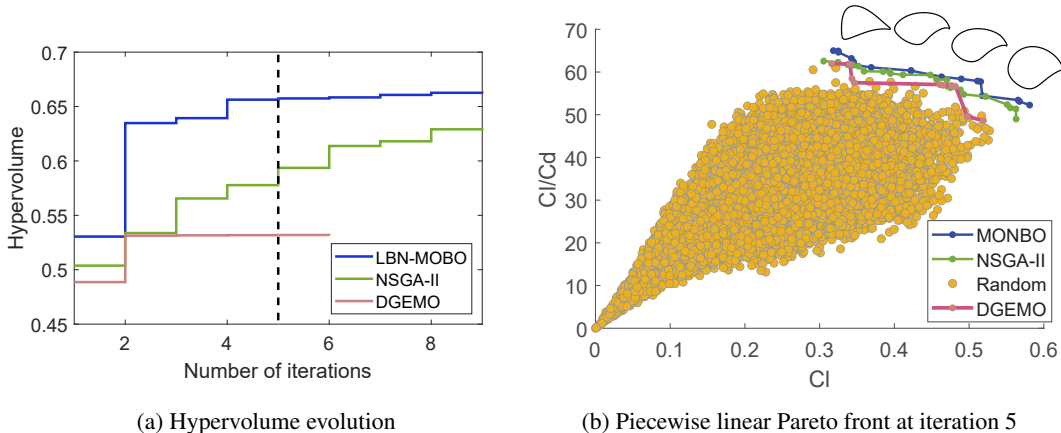


Figure 4: The hypervolume evolution and the Pareto front of the airfoil problem of LBN-MOBO and NSGA-II with equal batch sizes.

performance in ZDT3, although we must limit its batch size to 1,000 and restrict it to 5 to 6 iterations due to prohibitive run time.

Figure 4 showcases a comparison between NSGA-II, DGEMO, and LBN-MOBO for the airfoil problem. This experiment has a significantly more complex NFP since the relationship between the design and performance space is highly complex as we map the latent code of a GAN to aerodynamic properties. We start LBN-MOBO and NSGA-II with 15,000 samples, and each iteration runs with a batch size of 15,000 all simulated by OpenFOAM, a high-fidelity CFD solver [24].

Once again, as depicted in Figure 4a, LBN-MOBO discovers a superior Pareto front in a remarkably small number of iterations. Although with many more iterations, NSGA-II also reaches an acceptable Pareto front, this is most likely due to the use of a large batch size for each iteration in a comparatively smaller design space (five dimensions). In contrast, DGEMO’s performance significantly deteriorates. This likely stems from its reliance on the precise estimation of the gradient and Hessian of the NFP through the surrogate model. This task becomes increasingly difficult as the complexity of the NFP increases. In Figure 4b we show also the random samples to depict the landscape of performances.

For the task of exploring the 44-ink color gamut, we initialize LBN-MOBO with 10,000 samples, and each subsequent iteration processes a batch size of 20,000 samples. Given the high dimensionality of the design space, this problem poses a significant challenge to many optimization algorithms, making it a fascinating experimental case. The performance space in this experiment is the 2 dimensional $a*b$ color space. Figure 5a graphically depicts the accelerated increase in hypervolume of the color gamut when using LBN-MOBO. Also, final gamut estimation for NSGA-II and LBN-MOBO after 10 iterations, and DGEMO after 5 iterations, is depicted in Figure 5b, showing a significantly larger estimated gamut by LBN-MOBO.

4.4 The impact of uncertainty on the performance of LBN-MOBO

We investigate the impact of uncertainty on the computation of the Pareto front for both airfoil design and color gamut exploration. Both experimental setups mirror the conditions described in Section 4.3, except that they exclude uncertainty information. The candidate distribution from iteration 4 to 8 is illustrated in Figures 6a and 6b. For a clearer depiction of the samples’ spatial distribution, we have illustrated their convex hull. Note that in the absence of uncertainty, the candidates have a tendency to cluster within particular areas. This clustering leads to diminished diversity and, as a consequence, a reduction in the capacity for exploration (as represented by the yellow samples). Conversely, when uncertainty is incorporated into the process, we observe an increase in the diversity of the candidates and consequently, a broader Pareto front is discovered (represented by blue samples). Furthermore, uncertainty guides the candidates to progressively bridge the information gap in the surrogate models, making them increasingly similar to the NFP. This factor further enhances the quality of the Pareto front retrieved through the LBN-MOBO process.

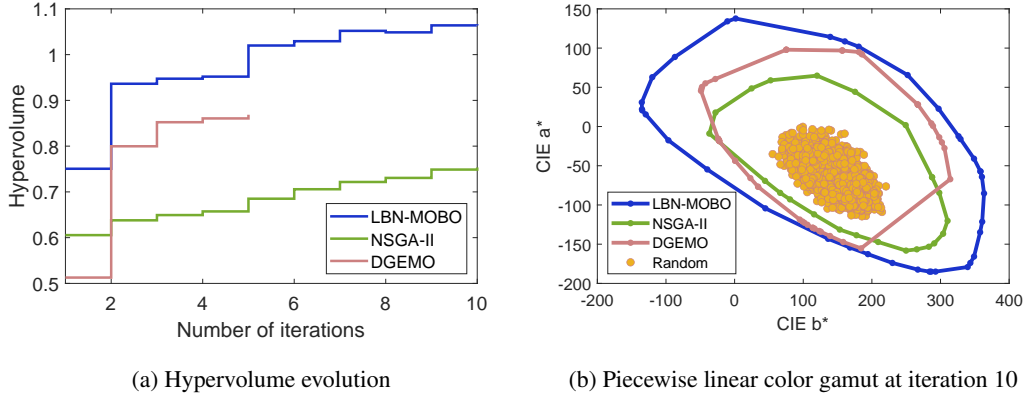


Figure 5: The hypervolume evolution and gamut of the 44-ink printer calculated by different methods.

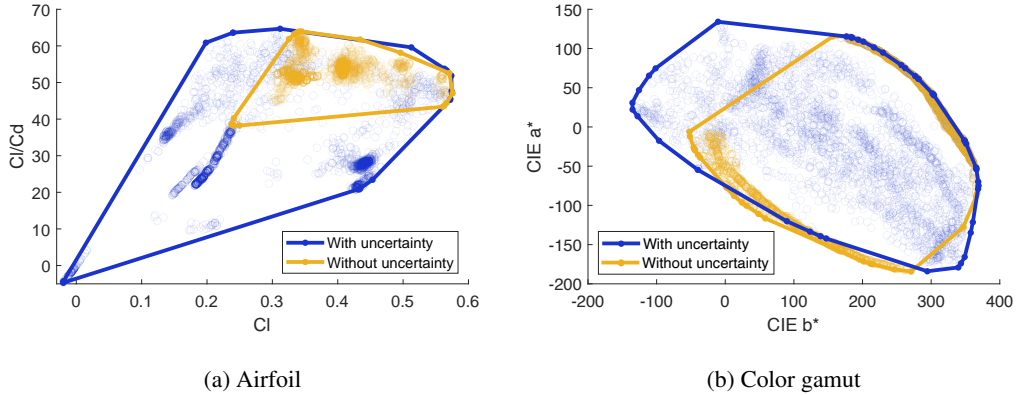


Figure 6: Ablation of uncertainty in our 2MD acquisition function.

We also observe that when uncertainty is excluded from the process, the budget for surrogate Pareto front optimization is concentrated solely on performance dimensions. This concentration may occasionally lead to a slight local enhancement in optimization, as illustrated in the bottom-left quarter of Figure 6b.

5 Discussion

LBN-MOBO emerges as a potent optimizer for problems where an increase in the batch size does not significantly inflate simulation or experimentation costs, but iterations are expensive. Notably, LBN-MOBO not only retrieves a superior Pareto front but also enhances the surrogate model throughout the optimization process, making it closely resemble the NFP. This implies that, within the context of active learning, this methodology could be implemented: starting with a random dataset and incrementally training the network with missing data until it converges to the NFP. Looking forward, there are a few key aspects of this method that warrant further exploration. First, the potential of LBN-MOBO in managing design constraints needs to be assessed. Second, an analysis of its performance in the presence of noisy data could be undertaken, and possibly, it could be extended to enhance its robustness against noise. Finally, while our current acquisition function is tuning-free, it is intriguing to explore explicit methods that manipulate the balance between exploration and exploitation and see how this balance affects the overall performance of LBN-MOBO.

References

- [1] Navid Ansari, Omid Alizadeh-Mousavi, Hans-Peter Seidel, and Vahid Babaei. Mixed integer ink selection for spectral reproduction. *ACM Transactions on Graphics (TOG)*, 39(6):1–16, 2020.
- [2] Navid Ansari, Hans-Peter Seidel, and Vahid Babaei. Mixed integer neural inverse design. *arXiv preprint arXiv:2109.12888*, 2021.
- [3] Navid Ansari, Hans-Peter Seidel, Nima Vahidi Ferdowsi, and Vahid Babaei. Autoinverse: Uncertainty aware inversion of neural networks. *Advances in Neural Information Processing Systems*, 35:8675–8686, 2022.
- [4] Frances H Arnold. Directed evolution: bringing new chemistry to life. *Angewandte Chemie International Edition*, 57(16):4143–4148, 2018.
- [5] Syrine Belakaria, Aryan Deshwal, Nitthilan Kannappan Jayakodi, and Janardhan Rao Doppa. Uncertainty-aware search framework for multi-objective bayesian optimization. In *Proceedings of the AAAI Conference on Artificial Intelligence*, volume 34, pages 10044–10052, 2020.
- [6] J. Blank and K. Deb. pymoo: Multi-objective optimization in python. *IEEE Access*, 8:89497–89509, 2020.
- [7] Eric Bradford, Artur M Schweidtmann, and Alexei Lapkin. Efficient multiobjective optimization employing gaussian processes, spectral sampling and a genetic algorithm. *Journal of global optimization*, 71(2):407–438, 2018.
- [8] Eric Brochu, Vlad M Cora, and Nando De Freitas. A tutorial on bayesian optimization of expensive cost functions, with application to active user modeling and hierarchical reinforcement learning. *arXiv preprint arXiv:1012.2599*, 2010.
- [9] Wei Chen and Faez Ahmed. Mo-padgan: Reparameterizing engineering designs for augmented multi-objective optimization. *Applied Soft Computing*, 113:107909, 2021.
- [10] George Cybenko. Approximation by superpositions of a sigmoidal function. *Mathematics of control, signals and systems*, 2(4):303–314, 1989.
- [11] Kalyanmoy Deb, Amrit Pratap, Sameer Agarwal, and TAMT Meyarivan. A fast and elitist multiobjective genetic algorithm: Nsga-ii. *IEEE transactions on evolutionary computation*, 6(2):182–197, 2002.
- [12] Kalyanmoy Deb, Lothar Thiele, Marco Laumanns, and Eckart Zitzler. *Scalable test problems for evolutionary multiobjective optimization*. Springer, 2005.
- [13] Nikita Durasov, Artem Lukoyanov, Jonathan Donier, and Pascal Fua. Debosh: Deep bayesian shape optimization. *arXiv preprint arXiv:2109.13337*, 2021.
- [14] Clara Fannjiang and Jennifer Listgarten. Autofocused oracles for model-based design. *Advances in Neural Information Processing Systems*, 33:12945–12956, 2020.
- [15] Yarin Gal and Zoubin Ghahramani. Dropout as a bayesian approximation: Representing model uncertainty in deep learning. In *international conference on machine learning*, pages 1050–1059. PMLR, 2016.
- [16] Richard Hague, Philip Dickens, and Neil Hopkinson. *Rapid manufacturing: an industrial revolution for the digital age*. John Wiley & Sons, 2006.
- [17] Kam Hamidieh. A data-driven statistical model for predicting the critical temperature of a superconductor. *Computational Materials Science*, 154:346–354, 2018.
- [18] Joel Hestness, Sharan Narang, Newsha Ardalani, Gregory Diamos, Heewoo Jun, Hassan Kianinejad, Md Patwary, Mostofa Ali, Yang Yang, and Yanqi Zhou. Deep learning scaling is predictable, empirically. *arXiv preprint arXiv:1712.00409*, 2017.

- [19] Kurt Hornik. Approximation capabilities of multilayer feedforward networks. *Neural networks*, 4(2):251–257, 1991.
- [20] International Commission on Illumination (CIE). *CIE 15:2004 Colorimetry*. CIE Central Bureau, 3rd edition, 2004.
- [21] Donald R Jones, Matthias Schonlau, and William J Welch. Efficient global optimization of expensive black-box functions. *Journal of Global optimization*, 13(4):455, 1998.
- [22] Mina Konakovic Lukovic, Yunsheng Tian, and Wojciech Matusik. Diversity-guided multi-objective bayesian optimization with batch evaluations. *Advances in Neural Information Processing Systems*, 33:17708–17720, 2020.
- [23] Balaji Lakshminarayanan, Alexander Pritzel, and Charles Blundell. Simple and scalable predictive uncertainty estimation using deep ensembles. *arXiv preprint arXiv:1612.01474*, 2016.
- [24] OpenFOAM Foundation. OpenFOAM. <https://openfoam.org/>, 2021.
- [25] Kyoungwoo Park and Juhee Lee. Optimal design of two-dimensional wings in ground effect using multi-objective genetic algorithm. *Ocean Engineering*, 37(10):902–912, 2010.
- [26] Adriana Schulz, Harrison Wang, Eitan Grinspun, Justin Solomon, and Wojciech Matusik. Interactive exploration of design trade-offs. *ACM Transactions on Graphics (TOG)*, 37(4):1–14, 2018.
- [27] Bobak Shahriari, Kevin Swersky, Ziyu Wang, Ryan P Adams, and Nando De Freitas. Taking the human out of the loop: A review of bayesian optimization. *Proceedings of the IEEE*, 104(1):148–175, 2015.
- [28] Simone. Hypervolume approximation. <https://www.mathworks.com/matlabcentral/fileexchange/50517-hypervolume-approximation>, 2023. MATLAB Central File Exchange.
- [29] Jasper Snoek, Oren Rippel, Kevin Swersky, Ryan Kiros, Nadathur Satish, Narayanan Sundaram, Mostofa Patwary, Mr Prabhat, and Ryan Adams. Scalable bayesian optimization using deep neural networks. In *International conference on machine learning*, pages 2171–2180. PMLR, 2015.
- [30] Raj Subbu, Piero P Bonissone, Neil Eklund, Srinivas Bollapragada, and Kete Chalermkraivuth. Multiobjective financial portfolio design: A hybrid evolutionary approach. In *2005 IEEE Congress on Evolutionary Computation*, volume 2, pages 1722–1729. IEEE, 2005.
- [31] William R Thompson. On the likelihood that one unknown probability exceeds another in view of the evidence of two samples. *Biometrika*, 25(3-4):285–294, 1933.
- [32] Nils Thuerey, Konstantin Weißenow, Lukas Prantl, and Xiangyu Hu. Deep learning methods for reynolds-averaged navier–stokes simulations of airfoil flows. *AIAA Journal*, 58(1):25–36, 2020.
- [33] Brandon Trabucco, Xinyang Geng, Aviral Kumar, and Sergey Levine. Design-bench: Benchmarks for data-driven offline model-based optimization. In *International Conference on Machine Learning*, pages 21658–21676. PMLR, 2022.
- [34] Günther Wyszecki and Walter Stanley Stiles. *Color science: concepts and methods, quantitative data and formulae*, volume 40. John wiley & sons, 2000.
- [35] Eckart Zitzler, Kalyanmoy Deb, and Lothar Thiele. Comparison of multiobjective evolutionary algorithms: Empirical results. *Evolutionary computation*, 8(2):173–195, 2000.

Appendix

A Implementation details

For our surrogate model, building on the methodology proposed in [3], we have constructed Deep Ensembles, utilizing a diverse collection of activation functions, to enhance the precision of epistemic uncertainty quantification. This enhancement serves as a cornerstone for ensuring the robust operation of the remaining procedures.

In our implementation, the deep ensemble comprises ten sub-networks, each employing a specific activation function as outlined below:

- Tanh $\times 2$
- ReLU $\times 2$
- CELU $\times 2$
- LeakyReLU $\times 2$
- ELU
- Hardswish

For the ZDT3 and printer’s color gamut networks, we employ a three-layer architecture, with neuron configurations of 100, 50, and 100 per layer respectively. To conduct our analysis on the rival methods, we utilized the pymoo library [6] and DGEMO source code [22].

Given the complexity inherent to the airfoil problem, it necessitates a more intricately designed network. We configured this network with four hidden layers, containing 150, 200, 200, and 150 neurons, respectively. In the Native Forwarded Process (NFP) of the Airfoil design, i.e., the open source fluid simulator OpenFoam, we have observed that sampling the latent space of the GAN near 0 and, in general, below 0.1 occasionally leads to invalid designs. This occurrence can introduce instability for the optimizers. To address this issue, we have imposed a limitation on the GAN latent space, restricting it between 0.1 and 1 to ensure the generation of valid designs.

Over the course of the LBN-MOBO iterations, data accumulation intensifies. Although it is feasible to progressively enlarge the batch size to maintain a constant total training time, we have chosen to keep the batch sizes fixed due to the minimal increment in training time relative to competing methods. Specifically, we employed a batch size of 20 for the airfoil problem, 10 for ZDT3, and 100 for the printer’s color gamut.

All networks underwent a training period spanning 60 epochs.

We leveraged a parallel compute cluster consisting of GPUs and CPUs for the simultaneous training of the network and computation of the acquisition function.

The GPU units within our cluster comprise two models: the NVIDIA Tesla A100 and the NVIDIA Tesla A40.

B Complementary experiments

B.1 More ZDT problems

In this section, we showcase ZDT1 and ZDT2, two problems from the ZDT test suite [35]. Both problems involve conflicting objectives, with the only distinction that ZDT1 has a convex Pareto front, whereas ZDT2 has a non-convex one. Both tests are conducted using their original 30-dimensional design space. The problem setup configuration is entirely identical to that of the ZDT3 problem Section 4.2 in the paper. As illustrated in Figure 7, similar to the case of ZDT3, LBN-MOBO demonstrates its superiority in both the ZDT1 and ZDT2 problems.

The Pareto front in Figure 7 for the ZDT1 problem was obtained after 10 iterations for all the methods considered in the analysis. As for the ZDT2 problem, USEMO and DGEMO were able to run for 7 iterations, while TSEMO managed to run for 8 iterations before becoming intractable.

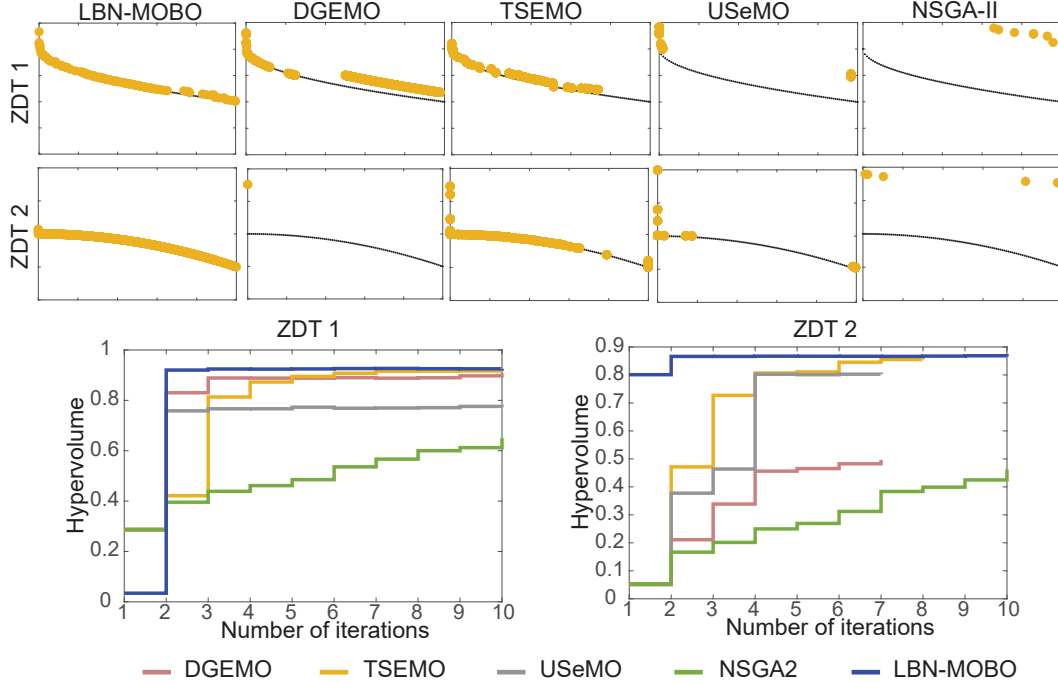


Figure 7: ZDT 1 and ZDT 2 in 30 dimensional setting. Note the immediate convergence of LBN-MOBO to Pareto front (bottom). The Pareto front is presented after 10 iterations of optimization except for USeMO (7 iterations), DGEMO (7 iterations), and TSEMO (8 iterations) in ZDT2 problem.

B.2 Performance of LBN-MOBO on DLTZ test suite with 3 objectives

In this section, we aim to compare the performance of our method on two problems from the DLTZ test suite [12] with a 6-dimensional design space and a 3-dimensional performance space. We address both the DLTZ1 and DLTZ4 problems using the same configuration described in the ZDT3 problem Section 4.2 of the paper.

Figure 8 illustrates that while LBN-MOBO has achieved the most diverse set of solutions, the performance of DGEMO and NSGA-II in locating solutions on the Pareto front has been superior. Here, USeMO missed a portion of the Pareto front, and TSEMO has largely failed in this regard.

On the contrary, Regarding the DLTZ1 problems, all the methods have shown a failure in generating a satisfactory Pareto front. However, upon analyzing the 2D projections, we discovered that our method was able to identify the Pareto front locally.

Figure 9 presents the 2D projections from three different angles, showcasing the results obtained by all the methods.

B.3 Printer color gamut for 8 ink

Figure 10 displays the results of the printer color gamut problem, which has a setup that is nearly identical to the 44-ink problem, with the exception that its NFP is trained using real data instead of synthetic data. The advantage of this NFP, is in its ability in accurately mimicking the behavior of the Epson printer from which the dataset is derived [1].

As observed, both NSGA-II and DGEMO exhibit results that are closer to LBN-MOBO, which could be attributed to the lower dimensionality of the problem.

C Complementary discussions

USeMO [5] shares some similarity with LBN-MOBO, however, besides its limitation in handling large batches, its utilization of uncertainty information is much more limited than ours. USeMO

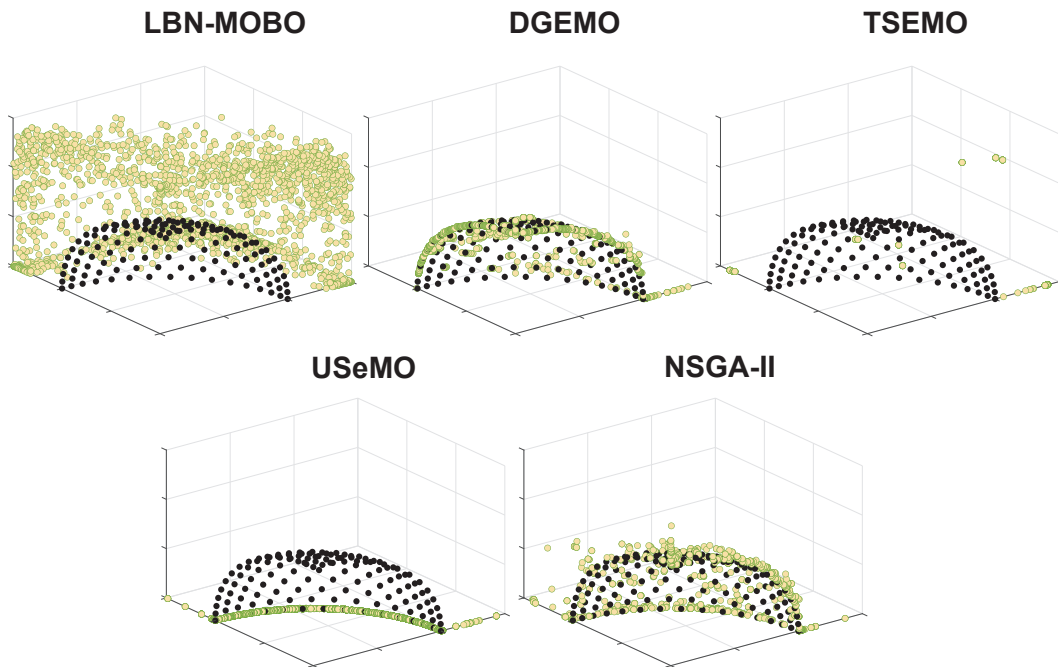


Figure 8: The paretofront of the DLTZ4 problem with 6-D input and 3-D output.

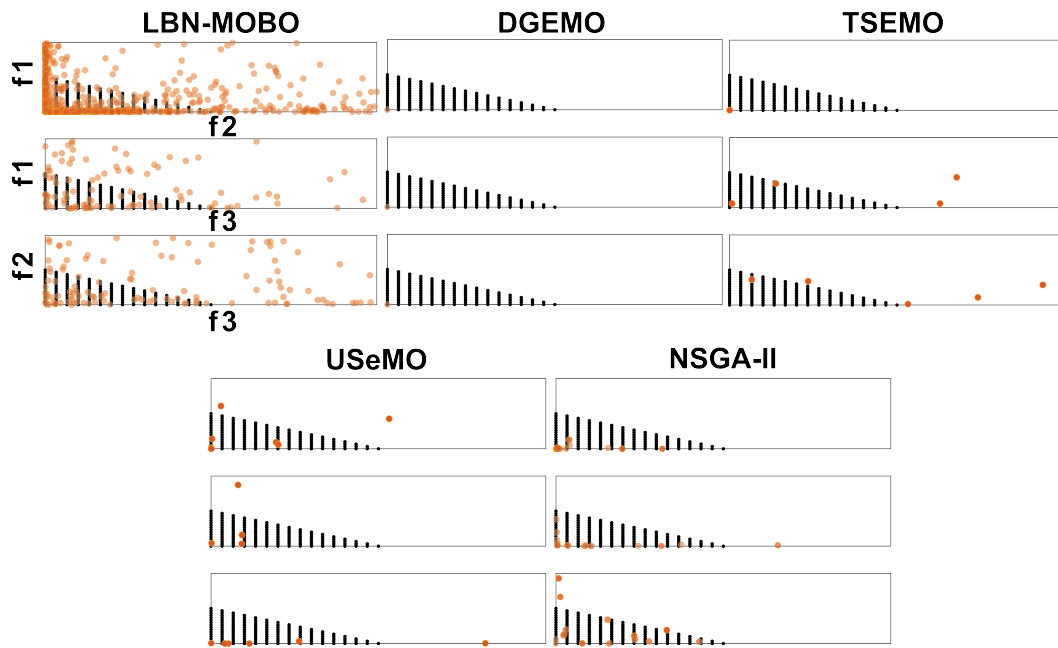


Figure 9: The 2-D projection of the paretofront of DLTZ1 problem with 6-D input and 3-D output.

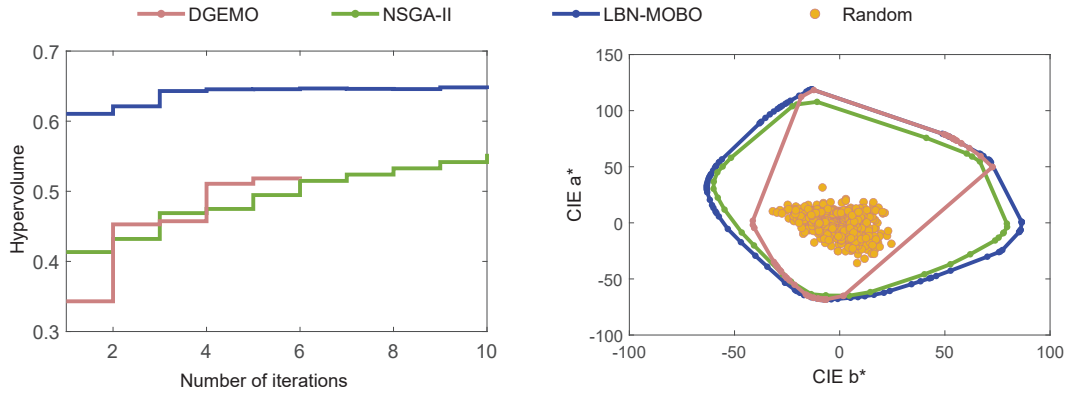


Figure 10: 8-ink printer gamut

finds the Pareto front on their surrogate function by running the NSGA-II [11]. Note that they do not optimize for uncertainty in a simultaneous manner as it happens in our $2MD$ acquisition. Instead they use uncertainty in a sequential manner to choose the most promising candidates among the ones already calculated by the NSGA-II. This approach cannot account for the samples that are not Pareto dominant according to performance predictions but have high uncertainty. As a result, they do not benefit from the advantages that we explained in Section 4.4 of the paper. The results in Figure 2 in the paper and Figures 7, 8, 9 in the supplementary materials also confirm that USeMO is not very successful in recovering a diverse Pareto front.

Similar to USeMO, TSEMO [7] utilizes NSGA-II for the calculation of the approximated Pareto set and Pareto front on the computationally inexpensive surrogates. What brings TSEMO closer to our approach is their utilization of Thompson sampling [31] to exploit or explore the black box function, guided by the uncertainty information obtained from Gaussian process surrogates.